AIAA JOURNAL
Vol. 41, No. 6, June 2003

Characterization of Aircraft Wake Vortices by Multiple-Lidar Triangulation

Friedrich Köpp,* Igor Smalikho,† and Stephan Rahm‡
DLR, German Aerospace Research Center, D-82234 Wessling, Germany
Agnès Dolfi§ and Jean-Pierre Cariou¶
ONERA, 91761 Palaiseau, France
and
Michael Harris,** Robert I. Young,†† Kevin Weekes,‡‡ and Neil Gordon§§
QinetiQ Malvern, Malvern, England WR14 3PS, United Kingdom

Three continuous-wave lidar systems have been deployed to measure simultaneously the airflow associated with wake vortices generated by a medium-size full-scale test aircraft. The lidar systems were positioned to permit investigation of fundamental aspects of vortex behavior. Two lidars were located 27 m apart, along a line parallel to the glide slope. This allowed a consistency check via comparison of the two sets of results and gave an indication of axial variations in vortex location and character. The third lidar was positioned 80 m away along a line perpendicular to the glide slope. This permitted accurate location of the vortex cores by triangulation methods via a tracking algorithm based on an extended Kalman filter, typically to an accuracy of better than ±4.0 m. The mean value of core separation for a vortex age of 2 s agrees to within 5% of that predicted for this aircraft using the approximation of elliptically distributed lift. Calculation of vortex circulation requires accurate information on vortex range in conjunction with tangent velocity profiles: The trajectories thus determined are an essential input, and, hence, this method will reduce the uncertainty in the values of circulation in comparison to studies involving only a single lidar.

Nomenclature

b_k	=	separation distance between the two vortex cores at time k
$\dot{b}_k$	=	rate of change of separation of the vortex cores at time k
$h_k^{1,i}$, $h_k^{2,i}$	=	state-to-measurement transformation functions for L_1 and L_2, respectively
i	=	index indicating either right r or left l vortex core
L_1, L_2, L_3	=	lidars of QinetiQ, ONERA, and DLR, respectively
$p(..)$	=	probability density function
t_k	=	time of the kth observation
w_k	=	Gaussian-distributed transition matrix noise term
x_k^m	=	horizontal position of the midpoint m between the two cores at time k
x_k^r, x_k^l	=	horizontal position of right, left vortex cores at time k
$\dot{x}_k^m$	=	horizontal velocity of the midpoint m at time k
y_k^m	=	vertical position of the midpoint m at time k
$\dot{y}_k^m$	=	vertical velocity of the midpoint m at time k
Δ_k	=	time elapsed since the last measurement
θ_k^1, θ_k^2	=	core elevation angle at time k for L_1 and L_2, respectively
$v_k^{1,i}$, $v_k^{2,i}$	=	Gaussian-distributed measurement noise term for L_1 and L_2, respectively
ϕ_k	=	angle of tilt between the vortices measured from the horizontal, defined to be positive when the left vortex core is higher than the right vortex core

Received 23 April 2002; revision received 2 January 2003; accepted for publication 10 January 2003.

*Research Scientist, Lidar Group, Institute of Atmospheric Physics, Oberpfaffenhofen; friedrich.kopp@dlr.de.
†Research Scientist, Lidar Group, Institute of Atmospheric Physics, Oberpfaffenhofen; igor.smalikho@dlr.de.
‡Research Scientist, Lidar Group, Institute of Atmospheric Physics, Oberpfaffenhofen; stephan.rahm@dlr.de.
§Research Scientist, Département Optique Théorique et Appliquée, Chemin de la Hunière; agnes.dolfi-bouteyre@onera.fr.
¶Manager, Laser Applications and Optoelectronics Unit, Département Optique Théorique et Appliquée, Chemin de la Hunière; cariou@onera.fr.
**QinetiQ Fellow, Sensors and Electronics Division, St. Andrews Road; mharris@qinetiq.com.
††Project Manager, Sensors and Electronics Division, St. Andrews Road; riyoung@qinetiq.com.
‡‡Research Scientist, Sensors and Electronics Division, St. Andrews Road; kweekes@signal.qinetiq.com.
§§Research Scientist, Sensors and Electronics Division; currently Research Scientist, Tracking and Sensor Fusion Group, Defence Science and Technology Organisation, P.O. Box 1500, Edinburgh, South Australia 5111, Australia; neil.gordon@dsto.defence.gov.au.

I. Introduction

COHERENT laser radar, also known as lidar, is a powerful technique for the detection and study of aircraft wake vortices. It relies on scattering of laser light from dust particles and other aerosols in the atmosphere, measuring their velocity via the Doppler shift. In a recent review,[1] we examined the range of lidar techniques that can be applied to the problems of vortex detection and monitoring; these issues have continuing relevance for aircraft design, air safety, and airport capacity.[2] The detailed structure and decay of full-scale vortices is most appropriately studied with continuous-wave lidar, by which method high resolution of airflow line-of-sight velocities is achieved.[1] Range resolution is achieved by focusing the beam at the desired distance, and the lidar typically collects scattering from an elongated region of space distributed about this point. Data are displayed as a sequence of spectra, with the outline of this pattern representing the radial variation of the tangential component of vortex velocity.[3] To first order, and with sufficient signal strength, the shape of this outline is independent of the focus range relative to the vortex cores. The outline can then be used for calculation of vortex parameters, such as circulation. Many such studies have been carried out previously, including those reported in Refs. 3–8.

A difficulty with earlier studies is the potential for large uncertainty in the calculated vortex parameters, brought about by the limited information available from a single lidar viewpoint. In particular, the inferred trajectories become increasingly unreliable as the vortex ages, especially in turbulent atmospheric conditions. Although accurate angular location of the vortex cores is generally easy to achieve, the range (that is, the distance between the lidar and the core) is usually subject to much greater uncertainty, so that the calculated trajectories contain large positional errors, elongated along the laser beam direction normal to the vortex core. These uncertainties translate directly to an error in the absolute physical size of the vortex structures and, hence, lead to proportional errors in the values of vortex circulation.

In this paper, we report measurements in which three lidar stations are used to probe simultaneously the vortices of a full-scale aircraft, DLR's Advanced Technologies Testing Aircraft System (ATTAS). The work represents a significant advance in such vortex investigations, in that it permits multiple nearly simultaneous views of the vortex flowfield. The core locations can be accurately determined using a tracking method based on triangulation (Sec. IV). Hence, the detailed vortex trajectories can be reconstructed, allowing in future publications a rigorous comparison with the results of ongoing modeling studies. The trial (WakeOP) was jointly realized by DLR's Wake Vortex Project, Wirbelschleppe, and the European program C-Wake during April and May 2001 at the Fairchild–Dornier Airfield and DLR Oberpfaffenhofen, Germany.[9] The campaign involved acquisition of additional meteorological data, for both the general area and the immediate locality, and two further lidars were deployed for the monitoring of local wind fields. Weather forecasting and wake prediction models were used to devise optimized flight plans and measurement scan patterns.

We restrict ourselves here to the analysis of the triangulation method as a means to reconstruct the vortex trajectories and make no attempt to correlate trajectories and decay of vortex circulation with meteorological conditions and aircraft configuration. Future papers will aim to cover some of these other interesting issues, including comparison with modeling data of vortex transport and decay. Section II. sets out the campaign geometry, including the lidar locations and scan patterns. Next, Sec. III demonstrates a consistency check that was performed on data from two of the lidars. In Sec. IV, we outline the triangulation analysis method, and some examples of the output from this analysis are presented in Sec. V. Finally, some discussion of the technique is presented in Sec. VI. Section VII provides a brief summary.

II. Measurement Procedure and Geometry

Details of the WakeOP campaign are given in Sec. VI of Ref. 9; we summarize the essentials here. The VFW 614 ATTAS aircraft with a span of 21.5 m and a typical weight of 19,000 kg falls toward the lower end of the medium-size category. It flew with prescribed configurations along optimized flight paths at speeds of around 60 m/s and altitudes of 150 m, thus avoiding vortex–ground effects. The aircraft's lateral position was chosen to maximize the time spent by the vortices within the area scanned by the lidars. The amount by which the flight path was laterally offset depended on the strength and direction of the crosswind. A total of 140 overflights took place on eight separate days; almost all flights allowed successful lidar measurement of vortex flows.

The day-to-day trial planning was greatly assisted by meteorological predictions provided by the application of a local forecast model, based on output from the German Weather Service. Direct measurements of wind speeds were carried out with monostatic and bistatic multiple-Doppler weather radar and with radiosonde launches. Local wind and other weather data were provided by a sodar radio acoustic sounding system, a pulsed 2-μm lidar for monitoring the runway crosswind component (described in Sec. II of Ref. 1), and a continuous 10-μm lidar located about 15 m from the QinetiQ lidar L_1, giving wind profiles and turbulence levels at five different altitudes up to 150 m. The input of the various wind data to a transport and decay model permitted prediction of wake trajectories and the optimization of flight paths. Finally, information from a lidar ceilometer on cloud ceiling proved valuable in the assessment of suitable conditions for lidar measurement.

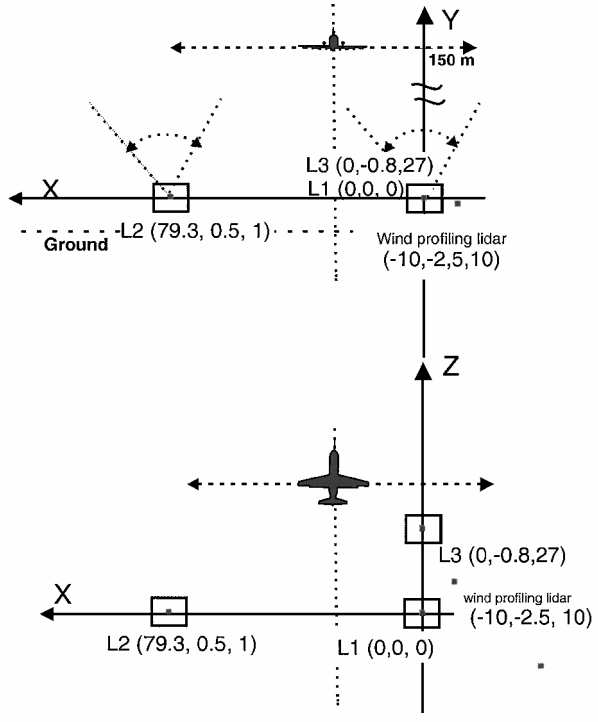

Fig. 1 Measurement geometry in plan and elevation; the precise aircraft trajectory and lidar scan patterns (range of angles and scan rates) were varied according to the prevailing weather conditions.

The three lidars used for vortex evaluation were of similar construction and performance, each emitting a continuous CO_2 laser beam of several watts at a wavelength of 10.6 μm via a telescope of 30-cm-aperture diameter. The lidar beams can be focused to ranges of up to ~200 m; optimum signal-to-noise ratios are obtained when the lidar is focused at the range of the vortex. The lidar beams are transmitted through optical scanners based on reflective optics, allowing accurate and reproducible beam pointing and scanning. The general principles of lidar operation and its application to vortex characterization are discussed in Refs. 1 and 3. Specific details of the individual lidars are presented in Refs. 4 and 5 and Refs. 3 and 7 for the DLR and QinetiQ lidars, respectively.

The measurement geometry in plan and elevation is shown in Fig. 1. The lidar locations are specified in terms of the positions of their scanner pivot points. The position of lidar L_1 (QinetiQ) is defined to be the origin (0, 0, 0) of the following coordinate system: 1) x is horizontal, perpendicular to the aircraft flight path; 2) y is vertical; and 3) z is horizontal in the direction of the flight path.

The height of the L_1 pivot above ground was 3.8 m. Lidar L_2 (ONERA) was located at (79.3, 0.5, 1.0) and L_3 (DLR) at (0, −0.8, 27.0), with the wind profiling lidar positioned approximately at (−10.0, −2.5, 10.0). The lidars were all scanned in the x–y plane. Because these scan planes are displaced with respect to each other, there is no possibility of interference between lidar returns (for example, light transmitted by L_1 being received by L_2).

Considerable care was taken in the calibration phase of the trial to ensure that all of the lidar scanners operated under the common coordinate system. Common absolute timing was also necessary for the correct implementation of triangulation. This was achieved by the use of time stamping derived from standard global positioning system receivers. The accuracy of the time stamping was checked by comparing the timing of a well-defined event (the blocking and unblocking of a Doppler target) that was clearly recognizable in the lidar output. Any discrepancy between lidars was measured to be less than 40 ms; timing errors of this order have a negligible impact on the triangulation results.

The lidar scan patterns were arranged to be constant in angular scanning rate (apart from small turnaround regions at the extremities

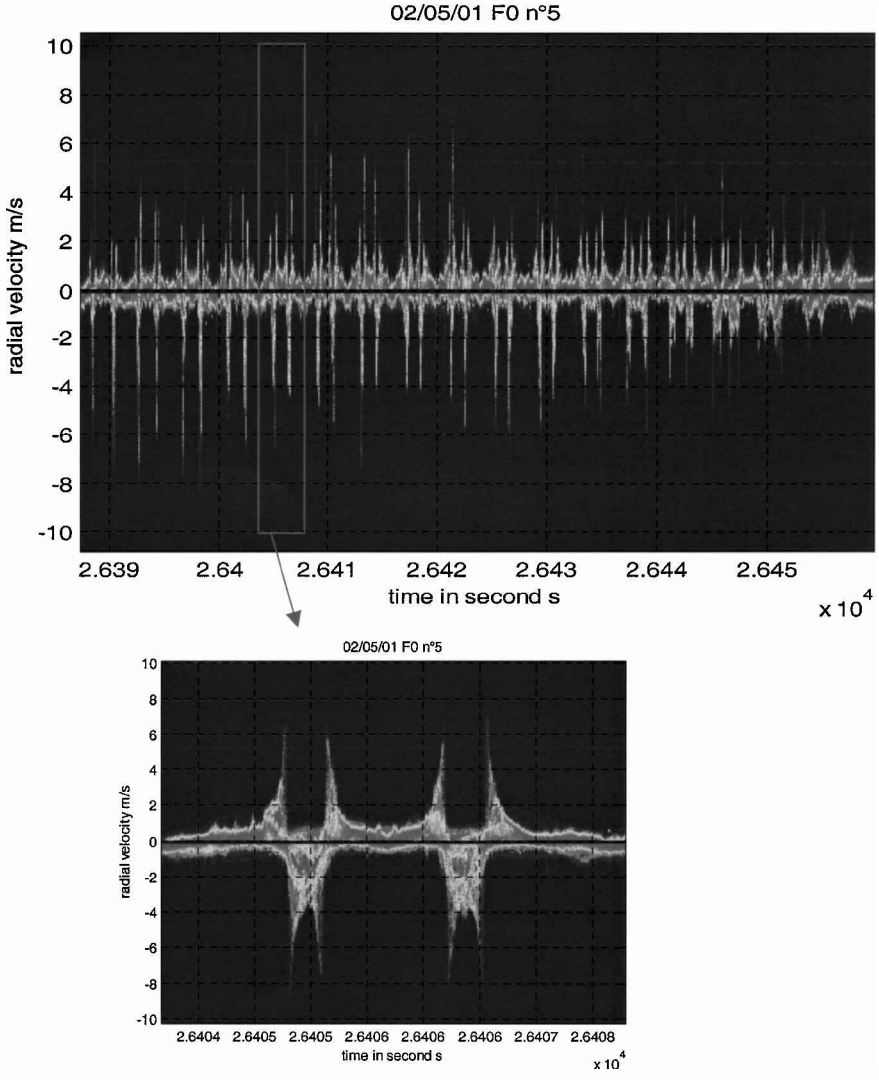

Fig. 2 Example trace from the ONERA lidar (L_2); the bottom part of the figure is an enlargement of the zone defined by the rectangular box, showing detail of the vortex pair.

of the scan), and the upper and lower angle limits were fixed throughout a particular run. For each flight, the chosen scan pattern depended on the aircraft trajectory, the prevailing weather conditions, and the measurement requirements. Typically scan ranges were of the order 30–50 deg, with scan speeds ranging from 5 to 25 deg/s. Faster scans give more intersections and better tracking of core location at the expense of reduced data quality for the individual vortex profiles. For the scan range, there is a similar tradeoff between the frequency of vortex interrogation and the dwell time of the vortices within the scanning area. No attempt was made to synchronize the lidar scan patterns: Each lidar operated independently of the others. Synchronization of lidar scans would bring about a considerable increase in complexity without any clear benefit. For the majority of flights, several vortex intersections were achieved with each lidar, and this is sufficient for the reconstruction of the vortex trajectories for at least some of the vortex lifespan.

An example of lidar spectral data is shown in Fig. 2, obtained for flight number 7#5 (denoting the fifth flight on day seven of the trial). The vertical scale represents the line-of-sight component of airflow velocity, with positive values indicating motion away from the lidar, that is, upward, and negative values motion toward the lidar. Each intersection of the laser beam with a vortex is clearly evident from the rapid change of sign as the beam traverses the core. Here, the favorable conditions and the relatively light crosswind (~0.4 m/s) combined with a rapid scan rate (25 deg/s) produces many vortex core intersections (~2 × 32). The series of velocity spectra has been acquired at a rate of 97.6/s, and the lidar was focused at ranges between 140 and 120 m. Subsequent analysis calculates the lidar scanner angle and absolute time for each intersection. The intersection angle/time data from the lidars then provide the input to the triangulation analysis tool, by which the trajectory of each core is calculated. The processing methods are discussed in Sec. IV.

III. Lidar Data Consistency Check

The availability of three lidar systems with similar performance offered the unique possibility to check the consistency of lidar results. As just indicated, lidars L_1 and L_3 were located along a line parallel to the flight direction, only 27 m apart from each other. The data simultaneously measured by these lidars are especially well suited for direct comparison of core positions. For this purpose, the elevation angles, where the scanning lidar beams were intersecting the cores of the vortex pair, have been derived from both sets of raw data. Two examples of direct comparison are shown in Fig. 3. In the case of flight 5#12, both lidars measured the left and right vortices starting from the position of aircraft passage near 90 deg, that is, the vortices are formed almost vertically above the lidars. Because of the vertical vortex descent, and driven by a moderate crosswind component, the vortices moved to lower elevation angles until they reached the boundaries of the scan regions near 42 deg for flight 5#12. Because the scanning regions of both lidars were set independently within different boundaries, there is only a limited time period of 2–10 s where data from both lidars are available. For case 8#11, the simultaneous measurements are covering the period from 2 to 19 s. The elevation angles are increasing from approximately

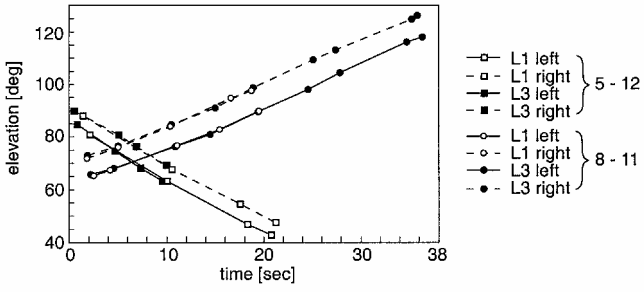

Fig. 3 Consistency check by comparison of vortex intersection data simultaneously measured by lidars L_1 and L_3: elevation angles of the left and right vortex cores for flights 5#12 and 8#11.

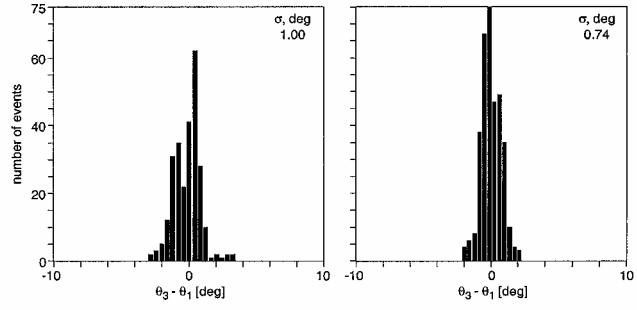

Fig. 4 Histogram of the differences of core elevation angles for 8 measurements of day 6 (left-hand side) and 10 measurements of day 8 (right-hand side).

70 to 90 deg because the aircraft passed at a lateral displacement of 84 m, and the crosswind component was approximately 4 m/s from opposite direction compared with case 5#12.

After linear interpolation between the measured events, the differences between the core elevation angles have been calculated in steps of 1 s. In Fig. 4, the differences for the left and right cores are combined in histograms for 8 cases from day 6 and 10 cases from day 8. They show very good agreement of the mean values to within less than 0.2 deg, with a standard deviation equal or less than 1 deg. Because a large part of this deviation can probably be attributed to fluctuations of the vortex position due to the 27-m distance between the scanning planes of lidars L_1 and L_3, the accuracy of the core elevation angles is within a fraction of a degree. This is the supposition for the reliable determination of vortex positions by means of the triangulation procedure. Besides the direct comparison of the elevation angles of core intersections presented earlier, it has also been possible to check the consistency of derivable parameters, like vortex trajectory, core separation, and vortex circulation.

IV. Triangulation Analysis

In this section, we briefly outline the method used to obtain vortex trajectories from multiple-lidar data. The purpose of using multiple lidars is to reduce the uncertainty in the vortex core locations by using triangulation to combine the results from two or more lidars. It is assumed here that two lidars are used simultaneously to probe the vortex pair and that each lidar scans in the vertical plane perpendicular to the direction of flight (Fig. 1). The two scanning planes are, therefore, parallel and closely spaced, and, hence, each lidar analyzes the same vertical slice of the aircraft's wake.

For each overflight, the lidars acquire data containing several intersections with at least one of the vortex pairs. These intersections give accurate angular information but poor range information. The two series of angular measurements (one from each lidar) can then be combined to produce the horizontal and vertical locations of the cores. These angular measurements are extracted from the raw wake spectra by using a vortex-profiling tool. The model used for the triangulation process is an extended Kalman filter (EKF),[10] in which the motions of the two vortex cores are considered to be linked to some degree. This linkage prevents the introduction of unphysically rapid variations in the trajectories, while permitting some degree of independent motion for the two cores allowing, for example, unequal left/right sink rates.

The EKF is a recursive nonlinear filter that is applicable for nonlinear models with additive Gaussian noise. It is a linearization technique based on a first-order Taylor-series expansion of the nonlinear system. Single-sensor bearings-only tracking is complicated by the lack of observability of range.[11] However, by the use of bearings from multiple sensors, it has been appreciated for some time that it is possible to triangulate,[12] potentially in difficult environments.[13] Applications include the tracking of submarines using passive sonobuoys,[14] as well as the deduction of depth from stereo images.[15] The linkage between the vortex cores allows the position of both cores to be updated whenever a core intersection is encountered, that is, both left and right core positions are updated regardless of whether the new intersection is from the left or the right core.

It is assumed that all of the processing is done at lidar L_1 and that there is no delay in communication between the two lidar stations. We assume the Cartesian framework outlined in Sec. II, with L_1 denoting the position of the QinetiQ lidar, situated at (0, 0, 0) and L_2 denoting the position of the ONERA lidar situated at (79.2, 0.5, 1.0). The dynamics of the system model are set up such that the required state vector is $\boldsymbol{X}_k = (x_k^m, \dot{x}_k^m, y_k^m, \dot{y}_k^m, \phi_k, b_k, \dot{b}_k)^T$, where the superscript T denotes the transpose.

By the use of simple trigonometry, the position of the left or right vortex core can then be found for any time t_k. The coordinates of the left core at time t_k are given by

$$y_k^l = y_k^m + (b_k/2)\sin\phi_k \tag{1}$$

$$x_k^l = x_k^m + (b_k/2)\cos\phi_k \tag{2}$$

Similarly, the position of the right vortex core at time t_k is given by

$$y_k^r = y_k^m - (b_k/2)\sin\phi_k \tag{3}$$

$$x_k^r = x_k^m - (b_k/2)\cos\phi_k \tag{4}$$

The received measurements Y_k contain only bearing information. These bearings are measured from the horizontal in the usual convention (θ increasing in the anticlockwise sense). Because either lidar can receive a measurement, we have two possible situations for the measurement Y_k, that is,

$$Y_k = \begin{cases} \theta_k^1 & \text{if} \quad L_1 \quad \text{makes the measurement} \\ \theta_k^2 & \text{if} \quad L_2 \quad \text{makes the measurement} \end{cases} \tag{5}$$

The system model allows the transition of the state from one time step to the next and is considered to be a constant velocity model in the x, y, and b parameters and a random walk in the ϕ parameter. The system update model takes the following form:

$$\boldsymbol{X}_{k+1} = F_k \boldsymbol{X}_k + w_k \tag{6}$$

where $p(w_k) = N(0, Q_k)$, denoting a normal distribution with zero mean and covariance Q_k. The state transition matrix F_k is then given by

$$F_k = \begin{pmatrix} 1 & \Delta_k & 0 & 0 & 0 & 0 & 0 \\ 0 & 1 & 0 & 0 & 0 & 0 & 0 \\ 0 & 0 & 1 & \Delta_k & 0 & 0 & 0 \\ 0 & 0 & 0 & 1 & 0 & 0 & 0 \\ 0 & 0 & 0 & 0 & 1 & 0 & 0 \\ 0 & 0 & 0 & 0 & 0 & 1 & \Delta_k \\ 0 & 0 & 0 & 0 & 0 & 0 & 1 \end{pmatrix} \tag{7}$$

where $\Delta_k = t_k - t_{k-1}$, the total time elapsed since the last measurement.

The measurement model allows us to convert the measurements recorded in angle space into positions in Cartesian space. Because there are two lidar stations measuring the vortex pair, there exist two

measurement models. The measurement models are considered to have the following forms:

$$Y_k = h_k^{1,i}(\boldsymbol{X}_k) + v_k^{1,i} \tag{8}$$

for sensor L_1 and

$$Y_k = h_k^{2,i}(\boldsymbol{X}_k) + v_k^{2,i} \tag{9}$$

for sensor L_2. The index i indicates from which target (core) we are currently processing the data. The additive noise models $v_k^{1,i}$ and $v_k^{2,i}$ are assumed to be Gaussian in form with $p(v_k^{1,i}) = N(0, R_k^{1,i})$ and $p(v_k^{2,i}) = N(0, R_k^{2,i})$.

Let (x_0, y_0) be the offset of lidar L_1 from lidar L_2. The state-to-measurement transformation function $h_k^{1,i}(\boldsymbol{X}_k)$ for sensor L_1 then takes the following forms:

$$h_k^{1,l}(\boldsymbol{X}_k) = \tan^{-1}\left(\frac{y_k^l}{x_k^l}\right) = \tan^{-1}\left[\frac{y_k^m + (b_k/2)\sin(\phi_k)}{x_k^m + (b_k/2)\cos(\phi_k)}\right] \tag{10}$$

for measurements made on the left core and

$$h_k^{1,r}(\boldsymbol{X}_k) = \tan^{-1}\left(\frac{y_k^r}{x_k^r}\right) = \tan^{-1}\left[\frac{y_k^m - (b_k/2)\sin(\phi_k)}{x_k^m - (b_k/2)\cos(\phi_k)}\right] \tag{11}$$

for measurements made on the right core. When the offset between the two lidars are accounted for, the state-to-measurement transformation function $h_k^{2,i}(\boldsymbol{X}_k)$ for sensor L_2 can be written in a similar form:

$$h_k^{2,l}(\boldsymbol{X}_k) = \tan^{-1}\left(\frac{y_k^l - y_0}{x_k^l - x_0}\right) = \tan^{-1}\left[\frac{y_k^m + (b_k/2)\sin(\phi_k) - y_0}{x_k^m + (b_k/2)\cos(\phi_k) - x_0}\right] \tag{12}$$

for measurements made on the left vortex core and

$$h_k^{2,r}(\boldsymbol{X}_k) = \tan^{-1}\left(\frac{y_k^r - y_0}{x_k^r - x_0}\right) = \tan^{-1}\left[\frac{y_k^m - (b_k/2)\sin(\phi_k) - y_0}{x_k^m - (b_k/2)\cos(\phi_k) - x_0}\right] \tag{13}$$

for measurements made on the right vortex core.

To enable us to apply the EKF model to the data, we require a linear approximation of these measurement models. This is achieved by taking the derivative of the state to measurement functions with respect to all of the state variables. The linear approximations for the measurements made by lidar L_1 of the left vortex core, therefore, have the following forms:

$$\frac{\partial h_k^{1,l}}{\partial x_k^m} = \frac{-y_k^l}{\left(x_k^l\right)^2 + \left(y_k^l\right)^2} \tag{14}$$

$$\frac{\partial h_k^{1,l}}{\partial \dot{x}_k^m} = 0 \tag{15}$$

$$\frac{\partial h_k^{1,l}}{\partial y_k^m} = \frac{x_k^l}{\left(x_k^l\right)^2 + \left(y_k^l\right)^2} \tag{16}$$

$$\frac{\partial h_k^{1,l}}{\partial \dot{y}_k^m} = 0 \tag{17}$$

$$\frac{\partial h_k^{1,l}}{\partial \phi_k} = \frac{(b_k/2)x_k^l\cos(\phi_k) + (b_k/2)y_k^l\sin(\phi_k)}{\left(x_k^l\right)^2 + \left(y_k^l\right)^2} \tag{18}$$

$$\frac{\partial h_k^{1,l}}{\partial b_k} = \frac{\frac{1}{2}x_k^l\sin(\phi_k) - \frac{1}{2}y_k^l\cos(\phi_k)}{\left(x_k^l\right)^2 + \left(y_k^l\right)^2} \tag{19}$$

$$\frac{\partial h_k^{1,l}}{\partial \dot{b}_k} = 0 \tag{20}$$

Similar linearization results are required for $h_k^{1,r}$, $h_k^{2,l}$, and $h_k^{2,r}$ to perform the triangulation procedure. Once these equations are found, they form the basis of the EKF model, and the full trajectory can be built up by an iterative procedure.

The only remaining unknown parameters are the system noise covariance matrix Q_{kt} and the measurement noise covariance matrices $R_k^{1,i}$ and $R_k^{2,i}$. The system noise covariance matrix is set as

$$Q_k = \begin{pmatrix} \frac{\Delta_k^3}{3}\tilde{q}_1 & \frac{\Delta_k^2}{2}\tilde{q}_1 & 0 & 0 & 0 & 0 & 0 \\ \frac{\Delta_k^2}{2}\tilde{q}_1 & \Delta_k\tilde{q}_1 & 0 & 0 & 0 & 0 & 0 \\ 0 & 0 & \frac{\Delta_k^3}{3}\tilde{q}_2 & \frac{\Delta_k^2}{2}\tilde{q}_2 & 0 & 0 & 0 \\ 0 & 0 & \frac{\Delta_k^2}{2}\tilde{q}_2 & \Delta_k\tilde{q}_2 & 0 & 0 & 0 \\ 0 & 0 & 0 & 0 & \Delta_k\tilde{q}_3 & 0 & 0 \\ 0 & 0 & 0 & 0 & 0 & \frac{\Delta_k^3}{3}\tilde{q}_4 & \frac{\Delta_k^2}{2}\tilde{q}_4 \\ 0 & 0 & 0 & 0 & 0 & \frac{\Delta_k^2}{2}\tilde{q}_4 & \Delta_k\tilde{q}_4 \end{pmatrix} \tag{21}$$

where $\tilde{q}_i$ is set to be approximately the change in the first derivative of each base state in time period $\Delta_k = t_k - t_{k-1}$. The measurement noise is one dimensional and is estimated from the raw vortex data.

The final stage in the vortex location procedure is the smoothing of the filtered trajectories. This Kalman smoothing process[16] uses all of the available data from the whole measurement period and works by iterating backward through the data (from the last measurement to the first), reestimating the vortex trajectory at each time step. This is particularly useful because any features in the trajectory caused by local fluctuations in the measurements will be removed. The final output of the analysis consists of the locations of each vortex core in x and y as a function of time after overflight. Some examples of these trajectory data are presented in the next section.

V. Triangulation Results

Figures 5–7 show an example of the reconstructed trajectory for one of the overflights (flight 1#13). In Fig. 5, the scan angles from lidars L_1 and L_2, corresponding to intersections with the two vortex cores, are plotted as a function of time, referenced to flyover. The times, hence, correspond closely to vortex age, albeit with a small discrepancy resulting from any head or tail wind, which brings about axial drift of the vortices. These data provide the input to the triangulation algorithm, and the output is displayed in Figs. 6 and 7. Figure 6 shows the motion of the vortex pair, with the indicated

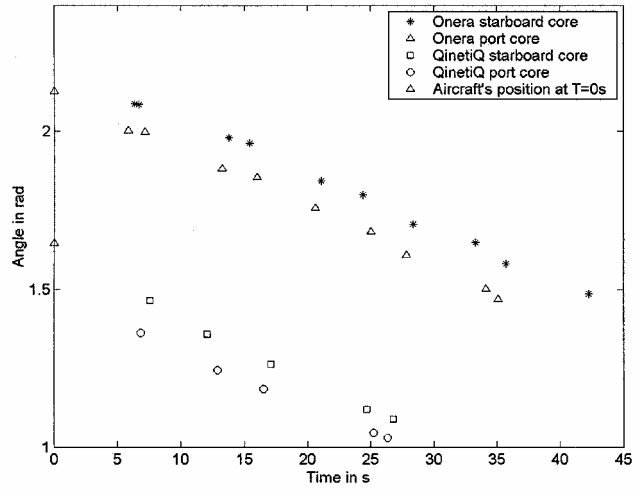

Fig. 5 Example (flight 1#13) showing the angles and timing of the intersections observed by lidars 1 and 2.

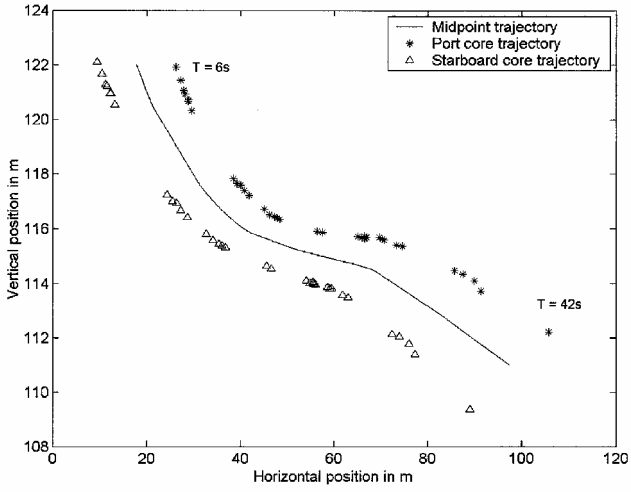

Fig. 6 Results from the triangulation method for flight 1#13, obtained under steady crosswind conditions.

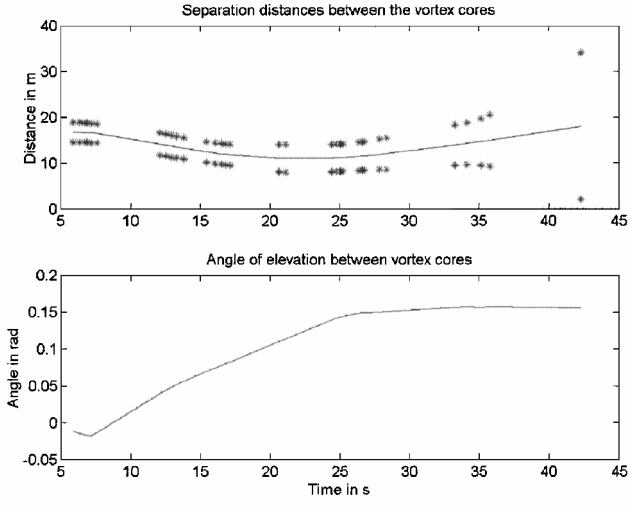

Fig. 7 Vortex separation b and angle of the line connecting the cores ϕ as a function of time for flight 1#13: $*$, 95% confidence limits.

times again relative to flyover. The derived trajectory of the vortex cores in the scan plane (perpendicular to the flight direction), are displayed. Figure 7 is a plot of the vortex separation b and the angle ϕ of the line connecting the vortex cores (relative to the horizontal) as a function of time. The information contained in Figs. 5–7 can be presented in a number of ways; note, however, that they contain all of the data required to plot the motion of the individual cores.

Several cross checks were performed to confirm the validity of the results. The altitude and lateral position of the aircraft were known to an accuracy of ~10 m through its onboard instrumentation. For the preceding example, the aircraft coordinates are plotted in Fig. 5 and show good consistency with the lidar data. The lateral drift of the vortices in the crosswind can also be checked against the value measured by the wind profiler lidar and the 2-μm pulsed lidar. These gave values (averaged over the period during which the vortices were observed) of 2.7 and 2.5 m/s, respectively. From Fig. 6, the vortices are transported 80 m over a time period of approximately 36 s, giving a mean drift velocity of 2.2 m/s, in reasonable agreement with the measured crosswind.

A second example of vortex trajectories is plotted in Fig. 8 (flight 7#5). This example has been chosen to illustrate an interesting trajectory. Modeling work is in progress to establish whether this trajectory is consistent with the predictions based on knowledge of the meteorological conditions for this measurement. The considerable variations of the angle ϕ observed in the preceding examples are typical. It is well established that unequal sink rates are likely for the two vortex cores in conditions where shear is present in the ambient

Table 1 Measured values of core separation b, averaged over the 48 analyzed flights

Vortex age, s	Mean core separation b, m	Standard deviation σ, m
$T = 2$	16.3	± 1.1
$T = 10$	17.8	± 2.3
$T = 20$	18.9	± 3.8
$T = 30$	20.9	± 7.2

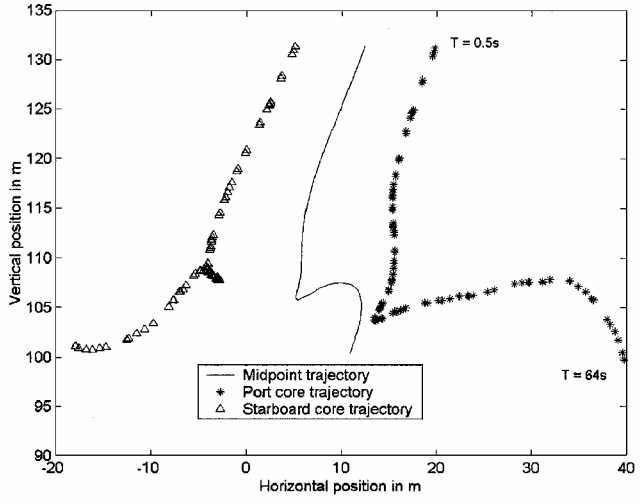

Fig. 8 Further example of the derived trajectory obtained under calm, stably stratified conditions (flight 7#5).

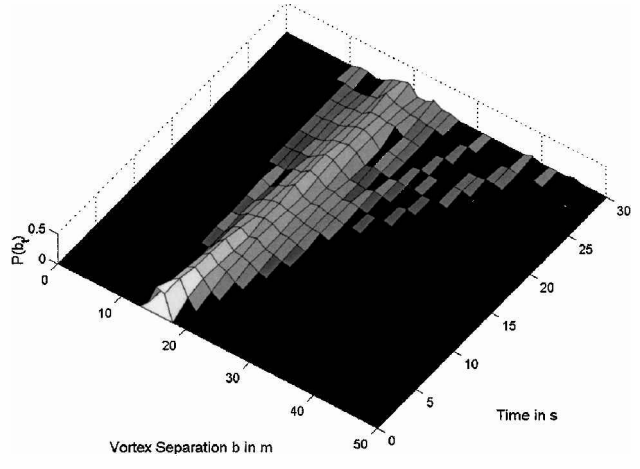

Fig. 9 Contour plot of core separation b as a function of vortex age; slice through the distribution at a given time represents a histogram of the values of b for that vortex age.

wind field.[9] The triangulation method provides an opportunity to measure these unequal sink rates; with single lidar measurements, it is difficult to define the angle ϕ with any degree of accuracy.

An important output of the triangulation analysis is the measurement of vortex separation b. This parameter is not only of direct interest for determining vortex trajectory and decay, but it also permits the best opportunity at WakeOP for an absolute comparison between prediction and a measured vortex property. The predicted value for the ATTAS aircraft using the approximation of elliptically distributed lift is $b = 16.9$ m. Figure 9 shows a contour plot of vortex separation b against vortex age for the 48 analyzed flights.

There is a clear trend toward a larger spread in b as time increases, and the mean value also increases slightly. These trends are quantified in Table 1. Note that the measurement uncertainty for b does not alter significantly over the vortex timescale considered. The increase in scatter for b is, therefore, a genuine effect, brought about by the unpredictable influence of the atmosphere. We also conclude that the apparent increase in mean b is real, and the reasons for this

are the subject of current debate. Simple calculations show that, for the conditions of the WakeOP trial, vortex–ground interaction can not be responsible for the increase in b. The value of b at $T = 2$ s agrees to within 4% of the elliptical-load prediction of 16.9 m. The corresponding standard deviation of ± 1.1 m must be taken as an upper limit for the measurement error in b because it will include additional contributions from the atmosphere and also from the actual spread in b caused by the different aircraft configurations used on the WakeOP trial. At present, it is not possible to give an accurate estimate of the likely deviations from the elliptical approximation for the ATTAS configurations. Overall, therefore, we conclude that the measurement error for b is probably smaller than 1 m, and this absolute error should still apply in the case of larger aircraft such as the A340, leading to a smaller percentage error in this case.

Next, we compare the results of a multiple-lidar tracking system with those of a single-lidar tracking system. In the multiple-lidar tracking system, core intersections from both lidar teams have been used, whereas in the single-lidar tracking system only the core intersections from the QinetiQ lidar are used. Both vortex trajectories are predicted by using the aforementioned EKF model. In the single-lidar case it is assumed that the ONERA lidar receives no measurements. By this method, we can demonstrate the reduction in error in core location for a multiple-lidar tracking system. To enable a fair comparison between the two methods, the noise covariance matrices are initialized at the same values.

Figure 10 shows the trajectory for a single-lidar tracking system for the example of flight 1#13 presented earlier, compared with the trajectory for the multiple-lidar system. The error ellipses represent 95% confidence levels, and they are seen in the multiple-lidar case to be of order ± 5–10 m. For the assumed Gaussian errors, the standard deviation σ is one-half of this value, and a more systematic analysis of the database reveals that σ is typically less than 4.0 m. A similar trajectory and errors are obtained for the starboard vortex. The error ellipses rapidly grow in size toward either end of the plot, particularly before L_1 and L_2 have both achieved their first intersection or after either L_1 or L_2 has observed its final intersection. Note that the single-lidar trajectory does not exhibit as much detail as the multiple-lidar trajectory. This is partly because the multiple-lidar system has more core intersections (measurements) and, thus, can predict the trajectory more accurately, and also because a single lidar cannot determine accurate range information. Therefore, in the single-lidar system, more emphasis is placed on the motion model and the initial starting values to determine the trajectory, resulting in the discrepancy in the core heights. Note from Fig. 10 that the multiple-lidar trajectory errors are much smaller than those produced by the single-lidar system. The single-lidar's errors grow as time increases, in contrast to the multiple-lidar system. This occurs because the single-lidar system has no means of correcting any errors made in the core locations, and, thus, the errors accumulate over time. The overall conclusion from this comparative error analysis is that multiple-lidar data allow the core positions to be located with an accuracy that is improved, typically by a factor of ~3 initially, rising to a factor of ~5 or greater after 30 s.

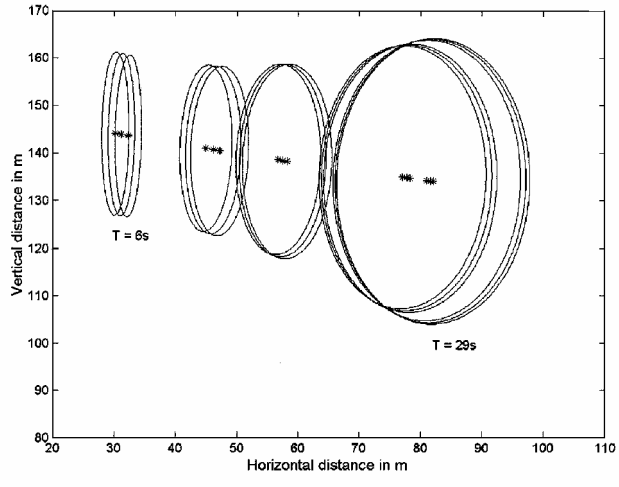

a)

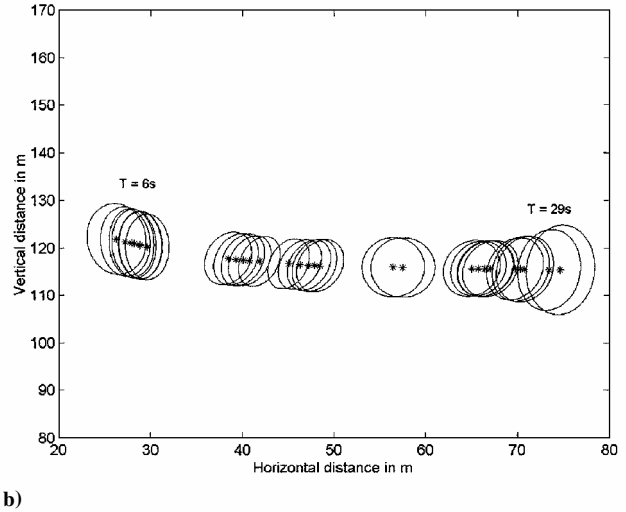

b)

Fig. 10 Trajectories for the port vortex core with associated uncertainty ellipses (95% confidence) (Fig. 6): a) single-lidar tracking system and b) multiple-lidar triangulation.

VI. Discussion

From the preceding analysis, we conclude that the multiple-lidar method reported here represents an advance for the accurate determination of vortex trajectories in full-scale flight trials. The typical uncertainty in core location is of order 4 m or less, and, in contrast with our earlier methods in which a single lidar is employed, the uncertainty does not necessarily increase with vortex age. The core separation b is defined to a greater accuracy of <1.1 m, and the values of b allow an absolute check of the method against expected vortex behavior. The relatively small aircraft size in these measurements must be borne in mind: It is hoped to apply the method to larger aircraft in future trials, and this should result in higher-quality data, resulting from the examination of a larger mass of air and a consequent reduction in percentage errors.

The accuracy of core location is significantly improved in comparison with that obtained by single-lidar measurements. For measurements such as those undertaken here, where repeated scanning through the vortex pair is necessary to evaluate the vortex lifecycle, the improvement is by a factor of order 3 to 5. Note, however, that considerably better single-lidar results can be achieved by employing careful range setting and by choosing special strategies, for example, waiting for vortex passage at preselected range gates, the so-called gate method.[4] This method allows definition of the vortex core position to ~5–10-m accuracy (depending on the range), but it does not generally permit repeated high-quality scans through the vortex pair.

An elegant alternative approach to reducing the uncertainty in vortex location has been developed by the group at Massachusetts Institute of Technology (MIT) Lincoln Laboratory under the Vortex Spacing System (AVOSS) project.[6,17] This method relies on active tracking of the vortex range by real-time analysis of the signal characteristics. The focus of the lidar is adjusted to optimize the overlap between the sensitive focal region and the vortex core, and the range to the vortex can then be inferred from the value of the lidar focus. It is instructive to compare the relative merits of multiple-lidar triangulation with this MIT system. The latter method has the obvious advantage that only one lidar is required. As well as the potentially lower cost, this also increases the deployability of the technique: There are considerable difficulties in identifying suitable sites where multiple lidars can be optimally located. On the other hand, the work presented here demonstrates the dramatic reduction in core location errors achievable by triangulation. These errors increase roughly linearly with vortex altitude when the baseline is of comparable length to the vortex altitude, whereas in the

MIT system, the increase is quadratic. This is likely to lead to considerably larger errors for a single lidar at altitudes above 200 m, seen as the most appropriate conditions for avoidance of vortex/ground interaction in studies of large aircraft. The MIT system assumes that the scattering particles (on which lidar relies to provide its signal) are uniformly distributed; in practice, entrainment of engine exhausts commonly produces inhomogeneities leading to the potential for increased errors. Finally, the feedback loop employed in active focusing necessarily involves the acquisition of data under degraded conditions for a significant fraction of the time. Approximately one vortex measurement in three is carried out under optimized focus conditions. In practice, therefore, the best choice will depend on many factors, including cost, site location, and desired measurement accuracy.

Future work will involve a full analysis of the WakeOP database in due course. This will allow more accurate statistical analysis of the various contributions to measurement uncertainty. Work is also in progress to correlate the measured trajectories with the meteorological data obtained at WakeOP.[9] The data describing the specific weather prevailing for each overflight can be used as input to models for prediction of vortex transport and decay and comparison with measured trajectories. In future trials, it is hoped that triangulation will be carried out using data from all three lidars located along a baseline perpendicular to the flight direction. Such schemes allow considerable flexibility, with a further reduction of core location errors and increased vortex observation time, especially in crosswind conditions.

A major overall aim of the WakeOP trial is the achievement of better characterization of the wake-vortex hazard to following aircraft. This requires calculation of the vortex circulation (requiring analysis of tangent velocity profiles) and its decay.[18] Results of this analysis will be presented in a subsequent paper. It is hoped that the improved core location brought about by triangulation will reduce many of the sources of uncertainty and reduce the overall scatter in values of circulation. Circulation values will also be compared for data obtained with different lidars on the same vortex. Such a comparison will give a reliable indication of the contribution of measurement uncertainty to the scatter in circulation. Finally, in cases where the vortex does not conform to our assumed axially symmetric model, we have the possibility to exploit the views from different directions afforded by multiple-lidar techniques.

VII. Summary

In summary, we have made, to our knowledge, the first multiple-lidar measurements of full-scale aircraft wake vortices. Detailed checks were performed to demonstrate the consistency of the measurements from two of the lidars. Triangulation analysis has been carried out leading to a significant reduction in the uncertainties for vortex core location. The inferred vortex trajectories display interesting features, and work is underway to correlate the observed behavior with measurement conditions and to validate models for vortex transport and decay.

Acknowledgments

We acknowledge cofunding of the activities by the C-Wake project within the Fifth Framework Programme of the European Union, by the CARAD program of the United Kingdom Department of Trade and Industry, and by the project Wirbelschleppe of DLR. We also gratefully acknowledge the essential contributions of all of the teams during the WakeOP trial: M. Klier and R. Simmet from the DLR lidar group; J.-P. Lafforgue, D. Fleury, D. Goular, and M. Jallot from ONERA; and G. Constant, R. Foord, J. Eacock, and P. Park from QinetiQ. From DLR Institute of Atmospheric Physics, we acknowledge T. Gerz, F. Holzäpfel, M. Frech, A. Tafferner, T. Hofbauer, T. Zinner, M. Hagen, K. Friedrich, R. Baumann, J. Freund, and W. Beer. From the Advanced Technologies Testing Aircraft System flight crew, we acknowledge H.-J. Berns, M. Press, A. Widmann, A. Knüppel, and O. Krüger. We are indebted to A. Münch and his team from Fairchild–Dornier for permission to use their airfield for this trial. Useful discussions were held with J. M. Vaughan of Microwave Management Associates and with R. Heinrichs and T. Dasey of the Massachusetts Institute of Technology Lincoln Laboratory.

References

[1]Harris, M., Young, R. I., Köpp, F., Dolfi, A., and Cariou, J-P., "Wake Vortex Detection and Monitoring," *Aerospace Science and Technology*, Vol. 6, 2002, pp. 325–331.

[2]Gerz, T., Holzäpfel, F., and Darracq, D., "WakeNet—The European Thematic Network on Wake Vortex: A Position Paper," URL: http://www.cerfacs.fr/~wakenet [cited 6 April 2001].

[3]Constant, G., Foord, R., Forrester, P. A., and Vaughan, J. M., "Coherent Laser Radar and the Problem of Aircraft Wake Vortices," *Journal of Modern Optics*, Vol. 41, 1994, pp. 2153–2173.

[4]Köpp, F., "Doppler Lidar Investigations of Wake Vortex Transport Between Closely Spaced Parallel Runways," *AIAA Journal*, Vol. 32, 1994, pp. 805–810.

[5]Köpp, F., "Wake-Vortex Characteristics of Military-Type Aircraft Measured at Airport Oberpfaffenhofen Using the DLR Laser Doppler Anemometer," *Aerospace Science and Technology*, Vol. 4, 1999, pp. 191–199.

[6]Joseph, R., Dasey, T., and Heinrichs, R., "Vortex and Meteorological Measurements at Dallas/Ft. Worth Airport," AIAA Paper 99-0760, Jan. 1999.

[7]Harris, M., Vaughan, J. M., Huenecke, K., and Huenecke, C., "Aircraft Wake Vortices: a Comparison of Wind-Tunnel Data with Field-Trial Measurements by Laser Radar," *Aerospace Science and Technology*, Vol. 4, 2000, pp. 363–370.

[8]Vaughan, J. M., and Harris, M., "Lidar Measurement of B747 Wakes: Observation of a Vortex Within a Vortex," *Aerospace Science and Technology*, Vol. 5, 2001, pp. 409–411.

[9]Gerz, T., "Wake Vortex Prediction and Observation: Towards an Operational System," *Proceedings of 3rd ONERA-DLR Aerospace Symposium (ODAS)*, ONERA, Chatillon, France, 2001, Chap. S1-3.

[10]Jazwinski, A. H., *Stochastic Processes and Filtering Theory*, Academic Press, New York, 1970.

[11]Lin, X., Kirubarajan, T., Bar-Shalom, Y., and Maskell, S., "Comparison of EKF, Pseudomeasurement Filter, and Particle Filter for a Bearing-Only Target Tracking Problem," *SPIE AeroSense Signal and Data Processing of Small Targets*, edited by O. Drummond, Society of Photo-Optical Instrumentation Engineers (International Society for Optical Engineering), Bellingham, WA, 2002, pp. 240–250.

[12]Lindgren, A. G., and Gong, K. F., "Position and Velocity Estimation Via Bearing Observations," *IEEE Transactions on Aerospace and Electronic Systems*, Vol. AES-14, No. 4, 1978, pp. 319–329.

[13]Kirubarajan, T., Bar-Shalom, Y., and Lerro, D., "Bearings-Only Tracking for Maneuvering Targets in Clutter," *IEEE Transactions on Aerospace and Electronic Systems*, Vol. AES-37, No. 3, 2001, pp. 770–780.

[14]Hernandez, M. L., "Efficient Data Fusion For Multi-Sensor Management," *Aerospace*, Inst. of Electrical and Electronics Engineers, New York, 2001.

[15]Yi, J. W., and Oh, J. H., "Recursive Resolving Algorithm for Multiple Stereo and Motion Matches, Image and Vision Computing," *Image and Vision Computing*, Vol. 15, 1997, pp. 181–196.

[16]Shumway, R. H., and Stoffer, D. S., *Time Series Analysis and Its Applications*, Springer Texts in Statistics 2000, Springer-Verlag, New York, 2000.

[17]Dasey, T. J., and Heinrichs, R., "An Algorithm for the Recognition and Tracking of Aircraft Wake Vortices with a Continuous Wave Coherent Laser Radar," *OSA Technical Digest Series, Vol. 19: Coherent Laser Radar*, Optical Society of America, Washington, DC, 1995, pp. 193–196.

[18]Holzäpfel, F., Gerz, T., Köpp, F., Stumpf, E., Harris, M., Young, R., and Dolfi, A., "Strategies for Circulation Evaluation of Aircraft Wake Vortices Measured by Lidar," *Journal of Atmospheric and Oceanic Technology* (to be published).

A. Plotkin
Associate Editor